A NEW GRID METHOD TO ANALYSE THE STAMPABILITY OF SHEET METALS BY CONCENTRIC CIRCLES PRINTED ON SURFACE OF THE MATERIAL

Ravilson Antônio Chemin Filho, Alex Raimundo de Oliveira,
Rafael Guetter Bohatch, Chetan Nikhare and Paulo Victor Prestes Marcondes

Abstract. *The production of automotive bodies for most vehicle models is carried out through sheet metal forming, a process capable of meeting the enormous demand in this segment. However, manufacturers face many challenges in terms of productivity, design, performance and safety, in addition to the process of electrifying cars, which also requires adaptation of models. To meet these needs, several studies have been carried out focused on modernizing car bodies, in terms of materials, processes and innovative projects. Within this context, however, with a focus on improving stamping processes, the Concentric Circles Method (CCM) was created in this study. The objective of the method is to improve investigative techniques regarding the effect of process and design variables in the stamping process on the behavior of plastic deformations. The model consisted of printing concentric circles on the surface of the test specimens used in the Modified Nakazima tests, which defined twelve regions on the sample, from the flange to the punch pole. Therefore, after stamping the DP600 steel until its rupture, the true deformations and Vickers microhardness in these regions were measured and calculated, from which representative graphs of the deformation and hardness profiles along the stamped sheet were obtained. These graphs allowed the precise interpretation of the effect of the sheet press forces (785 kN and 1157 kN) and the drawbead geometries (flat, circular and square) used in the tests, to explain the performance result obtained with the forming limit curves (FLC). Through the FLCs, a better stampability of the DP600 steel was achieved with the circular drawbead, in both blank holder forces (BHF), and a worse stampability performance with the flat drawbead (without the tooth), also with both BHF. As main conclusions, it was seen that the CCM method was effective and capable of explaining the stamping performance of DP600 steel obtained with FLCs, allowing a more sophisticated understanding of the material behavior during stamping, in addition to providing data for the improvement of numerical stamping simulation models.*

Keywords: Forming Limit Curve. Grid Analyses, Nakazima Test.

1. INTRODUCTION

The manufacture of automotive bodies involves the production of components with complex geometries, requiring detailed and precise engineering design in the development of stamping tools. To guarantee quality and efficiency in production, it is essential to consider a series of parameters that affect the stampability of materials, directly influencing the performance of the process and the formability of metal sheets. With the aim of meeting the demands of the automotive industry for lighter and safer vehicles, the steel industry has been challenged to develop new steel alloys with optimized properties, such as high strength and ductility, essential to guarantee structural integrity during manufacturing processes, especially when forming complex parts.

The manufacturing process of formed components, particularly in the automotive sector, crucially depends on stamping tools, or dies, which guarantee product quality. Researchers have focused on improving these tools, seeking solutions that result in high-quality products and reduced tryout time (adjustments and testing of tools). These investigations involve the detailed analysis of process variables, such as stamping speed, applied force, temperature and lubrication, factors that, when optimized, increase the efficiency and precision of the process, resulting in components with better finishing and shorter production times.

FLC (Forming Limit Curve):

The Forming Limit Curve (FLC), initially developed by Keeler (1965) [1], Goodwin (1968) [2] and Woodthorpe et al. (1969) [3], continues to be an essential tool for predicting the formability limits of metal sheets, allowing defects, such as fissures and cracks, to be identified before process failures occur. To assess FLC, the Nakazima test is widely used, consisting of a method standardized by ISO 12004-2 (2008) [4]. This test evaluates the behavior of the material under different states of deformation, using specimens with varying widths and printed with circular grids to monitor deformations. Recent studies, such as those by Hino et al. (2014), Pan et al. (2014), Schwindt et al. (2015), Cardoso et al. (2016), Paul (2021), Frohn-Sörensen et al. (2022), Oliveira et al. (2022), Sanrutsadakorn et al. (2021) and Rezazadeh et al. (2024) [5 -13], confirm the relevance of CLC in the evaluation and development of new materials and forming processes, showing that the Nakazima test is a reliable reference to characterize the formability limits of advanced high-strength steels used in industry automotive.

AHSS (advanced high-strength steels):

In recent years, the development of advanced high-strength steels (AHSS) has revolutionized industrial processes, especially in automotive manufacturing. The introduction of these new alloys has brought significant changes in forming parameters, requiring in-depth investigations into deformation mechanisms and the influence of stamping tools on material formability. Recent research has explored the use of new materials, such as dual-phase steels, and alternative processes to improve efficiency and reduce costs in the manufacturing of automotive parts. These advances are highlighted in the studies of Abeyrathna et al. (2015), Ke et al. (2018), Schmid et al. (2019), Barlo et al. (2019), and Sarand and Misirlioglu (2024) [14-18], which highlight the potential of these innovations to optimize production and meet the growing demands of the automotive sector. Another manufacturing process widely used in the automotive industry is welding, which directly affects the crystalline structure of materials. Khan et al. (2023), Rajak et al. (2023), Cheng et al. (2024) and Mansur et al. (2021) [19-22] in similar works investigate the hardness in the heat affected zone (HAZ) of dual-phase (DP) steels subjected to laser welding. Park et al. (2024) [23] investigated the effects of laser welding on the microstructure and mechanical properties of DP600 steel sheets with. The results demonstrate that the process preserves the strength and formability of the material, without compromising its structural integrity. These characteristics highlight the potential of laser welding in automotive applications that demand high mechanical strength and good formability, making it a viable and efficient option for the manufacture of structural components. This process influences both the strength and ductility of the welds, impacting the structural integrity of automotive components. The methodology adopted covers the analysis of different grades of DP steels, focusing on the behavior of the martensitic and ferritic phases, in addition to the influence of parameters such as heat input, chemical composition and thermal cycles.

Tool variables:

A relevant topic in research on mechanical forming is the analysis of the variables associated with stamping tools and their impact on the formability of materials. Parameters such as blank holder force, stamping speed, and lubrication conditions have been widely investigated to optimize the process, as demonstrated in the studies by Meng et al. (2014), Folle and Schaeffer (2017) [24-25], Schmid et al. (2019) [16], Paul et al. (2021) [9], Oliveira et al. (2022)[11], and Votava et al. (2023) [26]. Proper optimization of these variables not only increases process efficiency but also ensures that components meet the quality and performance requirements of the industry, especially in applications that demand high precision, such as automotive and aerospace.

Testing/measurement techniques:

Microscopy plays a key role in the detailed analysis of the microstructures of advanced high-strength steels (AHSS), such as DP 600, DP780 and TRIP940, allowing an in-depth understanding of the behavior of these materials in industrial processes. Advanced techniques, such as Light Optical Microscopy (LOM), Scanning Electron Microscopy (SEM) and Electron Backscatter Diffraction (EBSD), are widely used to investigate the distribution and interaction of phases such as martensite, bainite and ferrite. These tools are crucial for optimizing heat treatments and evaluating mechanical properties. Recent studies, such as those by Zhang et al. (2014) [27], Schwindt et al. (2015) [7], Ma et al. (2022) [28] and Sarand and Misirlioglu (2024) [18] highlight the importance of these techniques for modeling and understanding the deformation suffered by steel alloys, especially those applied in the automotive industry. These works analyze the impact of heat treatments on the microstructure of materials, revealing how differences between phases, such as ferrite and martensite, influence the non-uniform distribution of deformations, providing subsidies for the performance of these materials in industrial environments.

Furthermore, Lima et al. (2022) [29] proposed a new heat treatment with heating and holding temperatures adjusted to maximize bainite formation and minimize the presence of ferrite, seeking to improve mechanical properties without significantly increasing costs. Webber and Knezevic (2024) [30] investigated the strength of the ferrite and martensite phases in dual-phase (DP) and martensitic steels, respectively, with tensile strengths ranging from 590 to 1180 MPa. The authors correlated the local hardness of each phase with the global strength of the material, offering valuable insights for the development and application of AHSS alloys in industrial conditions. Katiyar (2024) [31] used the shot peening process on the surface of dual-phase (DP) steels with the aim of increasing wear resistance. The technique promoted stress-induced martensitic transformation and grain refinement, proving to be effective in improving both the mechanical and tribological properties of the material, contributing to applications that demand greater durability and strength. Shen et al. (2022) [32] carried out a comparative study between two steel alloys, one with high manganese content and the other of the two-phase DP1000 type. The research focused on the fracture toughness and mechanical properties of both alloys. The authors determined the Forming Limit Curves (FLC) through numerical simulations, which were validated with experimental tests, highlighting the effectiveness of the method in predicting the mechanical behavior and formability of the analyzed alloys.

The mechanical forming process, especially stamping, significantly changes the mechanical properties of the material during stamping. Among these properties, hardness stands out as one of the most impacted. During the process, the metal sheet is subjected to compression, promoting the hardening of the grains in its microstructure, which results in an increase in the hardness of the material. Automotive body components, whether cold or hot formed, present considerable changes in this parameter, which is crucial for assemblers and has been widely studied. Recent research, such as those by Shen et al. (2022), Lima T. et al. (2023) [33], Votava et al. (2023) [26], Sanrutsadakorn et al. (2023) [12], Nene (2023) [34], Rezazadeh et al. (2024) [13], and Sarand and Misirlioglu (2024) [18], explore the transformation of hardness in metal sheets and its impact on formability. To better understand these changes, several deformation analysis methodologies have been proposed, seeking to compare traditional models, such as Forming Limit Curves (FLC), with new methods that evaluate formability under nonlinear deformation conditions. In this context, the works of Pereira et al. (2024) [35], Katiyar (2024) [31] and Park et al. (2024) [23] provide valuable contributions to the development of more robust and accurate models, essential to optimize the manufacturing of automotive components.

Zhang et al. (2024) [36] developed an efficient methodology to model the hardening of materials with anisotropic mechanical properties, i.e., that vary in different directions. The approach uses experimental data and Finite Element Method (FEM) simulation. This methodology improves the prediction of plastic behavior in metals subjected to large deformations, offering a robust and accessible tool for industrial analysis, especially in forming processes and material optimization.

Tipalin et al. (2021) [37] investigated the impact of thickness on the hardening of the 12Kh18N10T sheet material, developing hardening curves and determining their coefficients. The research included detailed microhardness measurements along the thickness of the sheets, revealing a consistent pattern. And they state that hardness tends to decrease in the center of the material for different thicknesses analyzed and confirm the hypothesis that variations in hardness are directly related to the heterogeneous distribution of stresses and the microstructure throughout the thickness, contributing to the understanding of mechanical behavior in metal sheets.

Trzepiecinski (2020) [38] developed an innovative experimental method for the incremental forming of advanced high-strength steels. The study used a combined approach, applying controlled heating of these materials during the process and integrating numerical simulations based on the Finite Element Method (FEM). This methodology allowed a detailed analysis of the interactions between the forming parameters and the thermomechanical behavior of the steels, contributing significantly to optimizing industrial processes that demand high precision and efficiency in the formability of metal sheets.

Pereira et al. (2020) [39] developed a method for identifying parameters using hydraulic tests of circular and elliptical expansion. The methodology combines experimental data of pressure versus pole height with numerical simulations performed in the DD3IMP software. To optimize the hardening and anisotropy parameters, the Levenberg-Marquardt method was used, ensuring greater precision in the calibration of the models and contributing to the detailed analysis of the mechanical behavior of metal sheets in forming processes.

Krairi et al. (2020) [40] proposed the innovative Jump in Strokes method, designed to optimize numerical simulations in sheet metal cold forming processes. Applied to industrial components, such as AISI420 stainless steel and CR180B2 galvanized steel parts, the method uses Taylor expansion to extrapolate temperature fields between cycles, resulting in a reduction of up to 60% in computational cost. The approach has been experimentally validated in industrial processes, including sheet stamping for Philips and the manufacturing of automotive compartments for Opel, demonstrating high efficiency and accuracy. Furthermore, the use of advanced software for the correction of microstructure images has proven to be a powerful tool, allowing the elimination of distortions and improving measurement accuracy. This facilitates the quantification of microstructural phases and the detection of defects, contributing to a more accurate assessment of the behavior of materials under deformation. The combination of these techniques with numerical simulations and experimental tests has been essential for the development of more efficient and safer processes, as demonstrated by recent advances in the automotive industry in the use of AHSS and UHSS steels, as demonstrated by Abeyrathna et. al. (2015) [14].

The development of new steel alloys and the optimization of forming parameters, combined with the use of advanced microscopy and simulation techniques, are essential to meet the demands of the automotive industry for lighter, safer and more efficient vehicles, while ensuring quality and efficiency in the manufacturing processes of complex components.

2. MATERIALS AND METHODS

The material used in this study was Dual Phase 600 (DP600) steel, with a thickness of 1.0 mm, supplied by Siderurgica Usiminas S/A. This material was chosen because it is an AHSS steel, which has increasingly replaced traditional HSLA steels in structural components of automotive bodies. Based on this, studies aimed at a more sophisticated analysis of its behavior during stamping become feasible.

2.1 Mechanical properties and stampability parameters

The mechanical properties and stampability parameters were determined by tensile tests. The EMIC DL 3000 equipment was used, and the specimens were manufactured at the Machining Laboratory of the Federal University of Paraná, in accordance with the ASTM E8/E8M standard of 2016. The fundamental mechanical properties of the DP600 steel were obtained through the tensile tests: ultimate tensile strenght (UTS), yield strenght (YS) and total elongation (El). The stampability parameters of the steel were also determined: the anisotropy factor (r) and the work hardening expoent (n). These properties and stampability parameters are essential in the characterization of the material prior to the stamping tests, to verify the classification of the material according to its manufacturing standard and to determine the power law of the steel, which can be used as input in numerical simulation models.

2.2. Forming Limit Curve in the Stretching Region

Considering that the work in question is focused on a new analysis method, whose main variables are the force of the sheet press and the geometry of the drawbead, and the forming limit curve is an efficient parameter for quantifying the performance of steels for stamping, the test configuration was as follows:

Test specimens: the tests were limited to only four specimen dimensions, all with 200 mm in length and widths of 125, 150, 175 and 200 mm, as shown in Figure 1. Only these geometries were used, since these are the specimens that produce stretching deformations in the sheet metal, a condition in which the effect of the force of the blank press and the drawbead are predominant around the punch. The narrower specimens, whose sides do not have direct contact with the blank press and, therefore, produce deformations by drawing, were disregarded, since they do not allow a more precise evaluation of the effect of the force of the blank press and the geometry of the drawbead. It should be noted that, in practical operations, the drawbead acts fully on the entire contour of the part.

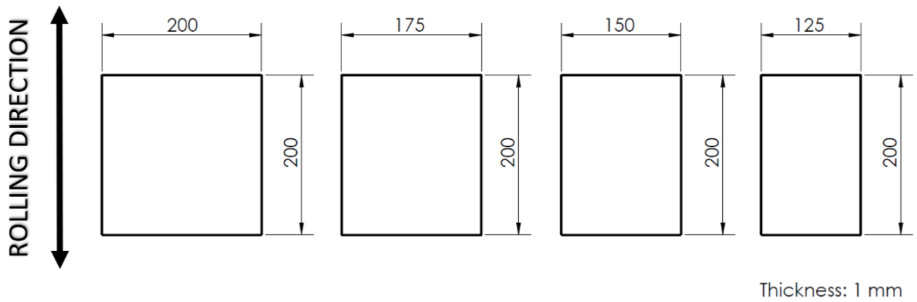

Figure1–Specimen’s geometry carried out on Modified Nakazima’s tests.

After the material was cut with a guillotine, the test specimens were cleaned and printed with a 5 mm diameter circle mesh using the silkscreen method. At this stage, the paint was prepared using a mixture of 90% epoxy paint and 10% nitric acid. This preparation ensured a good finish and good adhesion of the paint to the surface of the test specimens, i.e., the conditions required for accurate measurement of the sheet metal's planar deformations using the printed circle grid.

Tooling: the Modified Nakazima test tool proposed by Oliveira, et al (2022) [11], shown in figure 2, was used, from which the sheet was subjected to sheet press forces of 785 kN and 1157 kN, with flat (without the tooth), circular and square drawbead geometries, shown in figure 3.

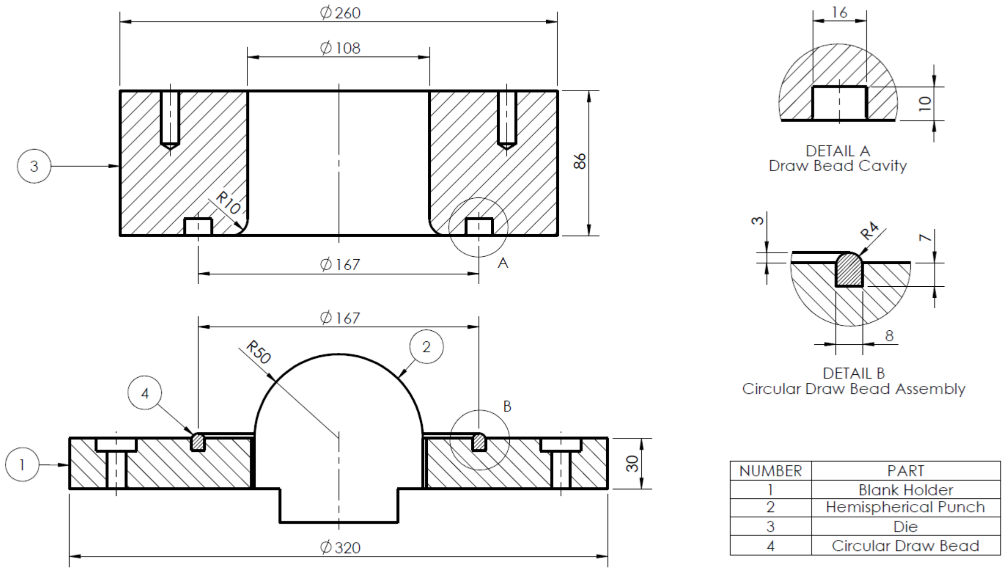

NUMBER	PART
1	Blank Holder
2	Hemispherical Punch
3	Die
4	Circular Draw Bead

Figure2–Modified Nakazima test tool with interchangeable drawbead rings.

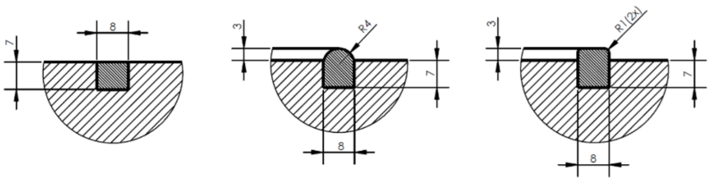

(a) (b) (c)

Figure3 – Details and dimensions of the drawbead geometries: a) flat drawbead, b) circular drawbead and c) square drawbead.

Except for the blank holder force and drawbead geometries, which were variables in the proposed tests, the other test parameters followed the ISO 12004-2 (2008) [4] standard.

2.3 New concentric circles model

In addition to the mesh mentioned above, concentric circles were printed on the upper face of the sample in the 200 x 200 mm test specimens, covering the punch pole, die radius and flange regions. This model was applied only to the 200 x 200 mm test specimens, in which there is uniform action of the plate press and drawbead throughout the punch contour. The other test specimens have a smaller contact area with the plate press in the width portion, where the sample dimension is smaller than the length, consequently affecting the material deformation gradient during stamping (non-uniform flow). The circles were drawn manually, using a precision compass and permanent marking pens.

The proposed diameters for the circles, as well as the colors used for each analysis region, are shown in Figure 4.

CIRCLES			DEFORMATION MEASUREMENT REGIONS
REGIONS	DIAMETER (mm)	COLOR	
Punch pole (stamping)	25,0	Red	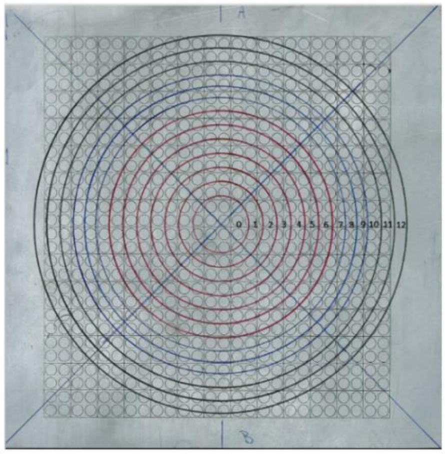
	37,5		
	50,0		
	62,5		
	75,0		
	87,5		
	100,0		
Die radius	112,0	Blue	
	122,0		
	132,0		
Flange	144,0	Black	
	156,0		
	167,0		

Figure 2–Dimensions and regions of the concentric circles printed on the sheet metal surface. Red circles on the punch pole region, blue circles on the die radius region and black circles on the flange region.

This model was proposed to measure deformations and microhardness region by region, from the flange, die radius, wall of the stamped body and punch pole, obtaining a variation profile of these properties along the stamped test specimen.

2.4 Measurement of deformations by region

The deformation of each of the regions indicated in Figure 4 corresponds to the variation in the distance between the circles that define each of them. Only the deformation of region zero (0), at the punch pole, is calculated by the variation in the diameter of the smallest circumference (diameter of 25.0 mm). Thus, there is an initial distance (d_{0n}) between the circles that define each region and, after the sheet is formed until rupture, the final distance (d_{fn}) is measured for each region. The measurements on the test specimen are taken along a straight line on the sheet, on the side opposite to the fracture of the material.

Thus, the conventional deformation of region 1, up to region 11, can be calculated by equation (1):

$$e_n = d_{fn} - d_{0n} \quad (1)$$

while the true deformation is calculated by the equation (2):

$$\varepsilon_n = \ln (1+e_n) \quad (2)$$

2.5 Microhardness analysis

To measure the Vickers microhardness in each region, the 200 x 200 mm test specimens, with the printed concentric circles, were cut in half, on the same line of deformation measurement, as shown in figure 5.

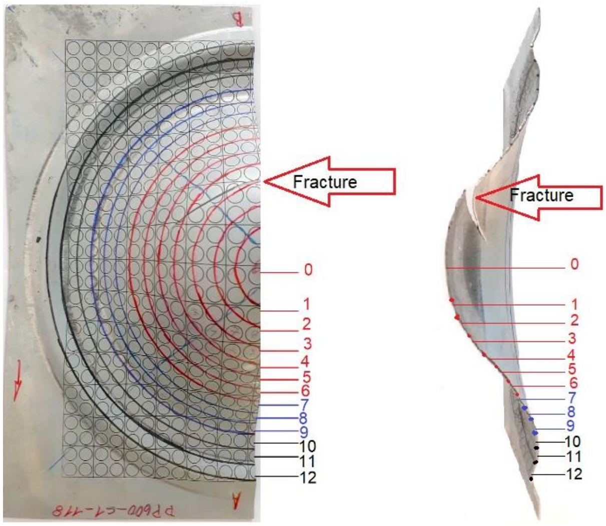

Figure5–200 x 200 mm specimen cutted on a straight line to the hardness measurement.

Smaller pieces were then cut in every three regions for embedding in bakelite and subsequent sanding and polishing. The embedded samples, duly prepared, were sent for microhardness measurement using a durometer (Shimadzu - HMV) in the materials laboratory at UFPR. A load of 200 g was used for the measurements. Three measurements were also taken in each region, one in the center and two others 1 mm to the right and 1 mm to the left of the first measurement. All measurements were taken at the center of the thickness of the embedded metal sheet.

3. RESULTS AND DISCUSSION

a. Fundamental mechanical properties and stampability parameters

Table 1 shows the mechanical properties and stampability parameters of DP600 steel. Results obtained from uniaxial tensile tests in different positions in relation to the sheet rolling direction (0°, 45° and 90°).

Table 1 - Mechanical properties and stampability parameters of DP600 steel.

Dual Phase 600 Mechanical Properties					
Rolling direction	Total elongation (%)	Uniform elongation (Mpa)	Ultimate tensile strength (Mpa)	Strain hardening exponent *(n)*	exponent of plastic anisotropy (r)
0°	27.8	375.4	658.9	0.9937	2.255
45°	24.1	378.1	664.8	0.8752	0.217
90°	26.1	356.4	657.1	12.188	0.2201
Average	26	370	660.3	10.292	0.2209

According to the results presented in Table 1, the material supplied for the work presented mechanical properties and stamping parameters as expected for the DP600, when compared to the data from (CITING AUTHORS).

Small variations in results between different batches of sheets supplied often indicate significant variations in the stamping tests, due to the great sensitivity of this manufacturing process to variations in sheet metal properties. Hence the need to perform preliminary tests to characterize the materials received.

b. Forming limit curves in the stretching region

From the stamping tests, conducted until the material ruptured, a total of six limit curves of forming of the DP600 steel were obtained, that is, one for each configuration between the two sheet press forces and the three available drawbead geometries. Thus, the curves were grouped in the same graph, for comparative analysis regarding the stampability of the sheet in each test condition, as shown in Figure 6. It should be noted that the result of the limit curves of forming is the basis for identifying, according to the characteristics of the deformation and hardness profiles, the causes that led to a better or worse performance of the material in each test configuration.

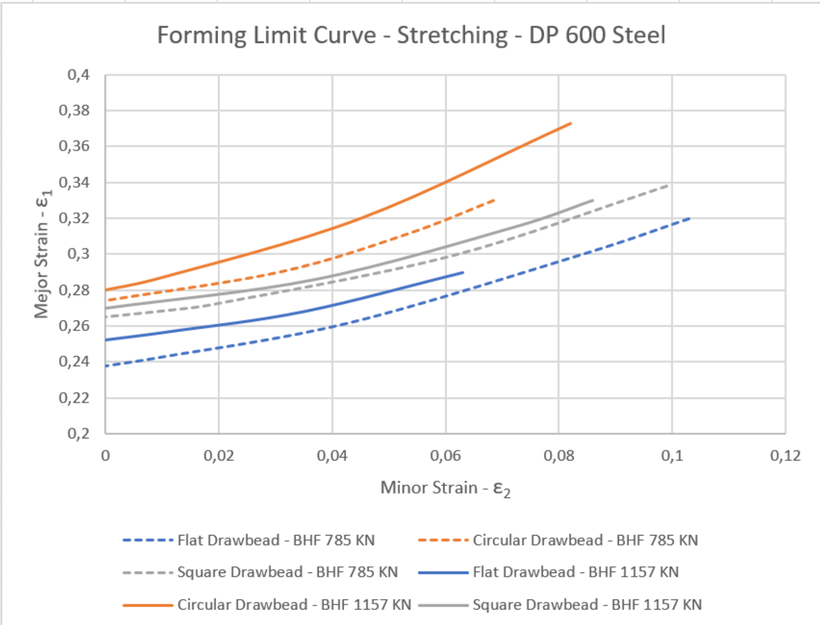

Figure6–Forming limit curves of DP600 steel on stretching region of the graphics.

Atenção as escalas nao é virgula e sim ponto.

According to the limit forming curves presented, the best performance with the circular drawbead and the worst performance with the flat drawbead are evident for both sheet press forces used. This result is very close to the results presented by Oliveira, et al (2022) [11], who performed similar tests for DP780 steel.

Another relevant result is that, analyzing each drawbead individually, all presented better performance with the sheet press force of 1157 kN, following the same results obtained by Chemin et. al (2011), also for DP600 steel. These results attest once again that, for very low sheet press forces, below a certain critical value, the yielding of the metal sheet becomes very accentuated and compromises the formability of the material.

In this way, it can be said that each drawbead has a very specific performance level, independent of the BHF, since, even though the performance of the circular DB with an BHF of 785 kN is lower than that of a force of 1157 kN, it was still superior to the best performance of the square DB, with a force of 1157 kN. The same happens if we compare the square DB with the flat one, as the FLC of the square DB with 785 kN was higher than the best performing FLC of the flat one, with 1157 kN.

In this way, the FLC clearly shows the real gains in sheet metal stampability with the use of drawbeads, in addition to how the use of a more appropriate tooth geometry and BHF can also increase the formability of the material.

In view of these results, the detrimental effect of the low restriction on the flow of the material in the flange region on its formability is evident, since the flat geometry, which less restricts the flow of the sheet during stamping, produced lower FLC curves. Thus, the restrictive function on the flow of the sheet, resulting from the use of the drawbead and the increase in BHF, substantially improves the formability limit of the material under study.

Through the analysis and discussion of the results in this chapter, it was observed that the best performance of the material, in terms of its formability limit, is achieved through the balance between BHF and drawbead geometry. Both variables imply a restriction on the flow of the sheet during stamping, and the interpolation between them is what determines the performance of the steel in the operation. However, a search for a more detailed explanation of the results is necessary. Therefore, a different model for analyzing stamping tests was sought, through which it would be possible to identify the real effects of the plate press force and the drawbead geometry on the results of the forming limit curves.

3.3 Sheet metal mechanics

For a more detailed analysis and a better understanding of the material's behavior during stamping, a study of the sheet mechanics during the forming process was carried out, through which we sought to identify the way in which the metal sheet deforms in certain regions along a section of the test specimen. Figure 7 shows the regions that were defined on the sample section, grouped along its profile.

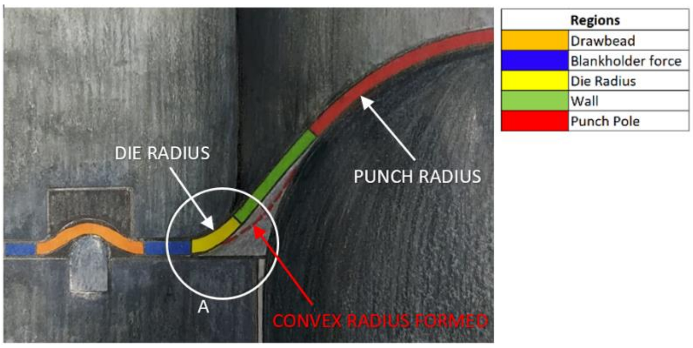

Figure 7 – Sheet metal mechanics during deformation.

In Figure 7, the blue regions represent the points where the force of the blank press acts directly on the material, between the flat surfaces of the die and the blank press. The orange region represents the deformed area of the sheet metal on the drawbead profile, still on the flange. At the end of the flange, in yellow, the folded region of the sheet metal on the radius of the die is represented, from which the sheet metal is already flowing into the tool. At this point, with the material subjected to the Bauschinger effect, the sheet metal bends in an anticlockwise direction (according to the orientation of the figure), a condition defined as “convex deformation” of the sheet metal.

From this point, the green region corresponds to the “wall” of the cup, and the red region to the pole of the punch. At the punch pole, the punch acts directly against the sheet metal, forming a pressure zone between the tool and the material, under intense friction, from which the sheet metal flows towards the wall region of the sample, that is, in the opposite direction to the flow of the sheet metal in the flange region, where it is pulled into the die. At the punch pole, the sheet metal is also curved in the opposite direction to the curvature over the die radius, forming a “concave” profile over the material.

Based on these characteristics, it can be said that the wall region, in an intermediate position between the die radius and the punch pole, is a friction-free zone, which represents an important transition in the flow direction and sheet curvature during stamping. Based on this, it can be said that the mechanical behavior of the sheet in the wall region is directly affected by the restrictive force on the sheet in the flange (defined by the force of the blank press and the geometry of the drawbead), which affects the flow of the material and, consequently, the degree of work hardening resulting from the bending of the sheet over the die radius.

The impact of the punch pole region on the wall region, which affects the flow of the material in this direction, depends only on the friction condition between the punch and the sheet, which, in laboratory tests, is constant. In practical terms, other variables must be considered, in addition to the lubrication condition, which affects the coefficient of friction, such as the geometry of the tooling (punch and die shape factor).

One characteristic, however, observed in the section of the stamped sheets was a third curvature along the sample profile, located at the beginning of the wall region, close to the region of the die radius (Figure 8). This curvature also presented a convex shape, as did the curvature of the sheet over the die radius, and was variable among the samples stamped with different BHF and DB geometries. This radius of curvature was not measured, however, its effect was evaluated based on the measurements of deformations and microhardness of the regions between the concentric circles.

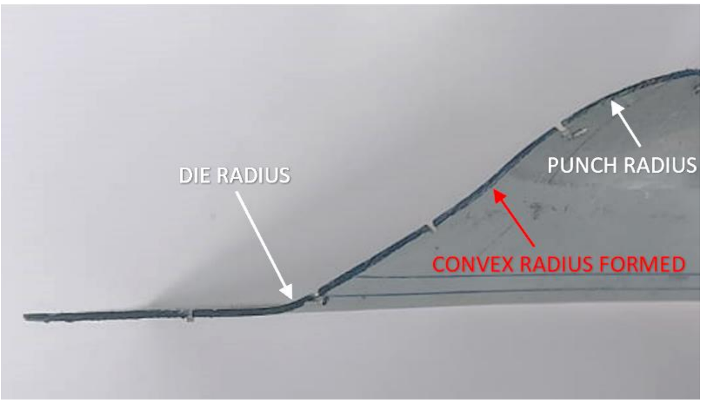

Figure 8 – Cross section of the specimen, with three radius formed by sheet metal strain.

Given the aspects mentioned, it can be said that the sheet wall region suffers a direct impact from the other regions of the sample profile during stamping. Therefore, a more detailed analysis of these effects on this region can explain the performance presented by DP600 steel through the forming limit curves.

3.4 Deformation profile between concentric circles

Figure 9 presents the graphs of true deformation as a function of the regions defined by the concentric circles (0 to 11), printed on the surface of the 200 x 200 mm samples, as illustrated in Figure 4. The curves were initially grouped for the blank holder forces of 785 kN and 1157 kN, figures 9(a) and 9(b), respectively, and, subsequently, for the flat, circular and square drawbeads, figures 9(c), 9(d) and 9(e), respectively.

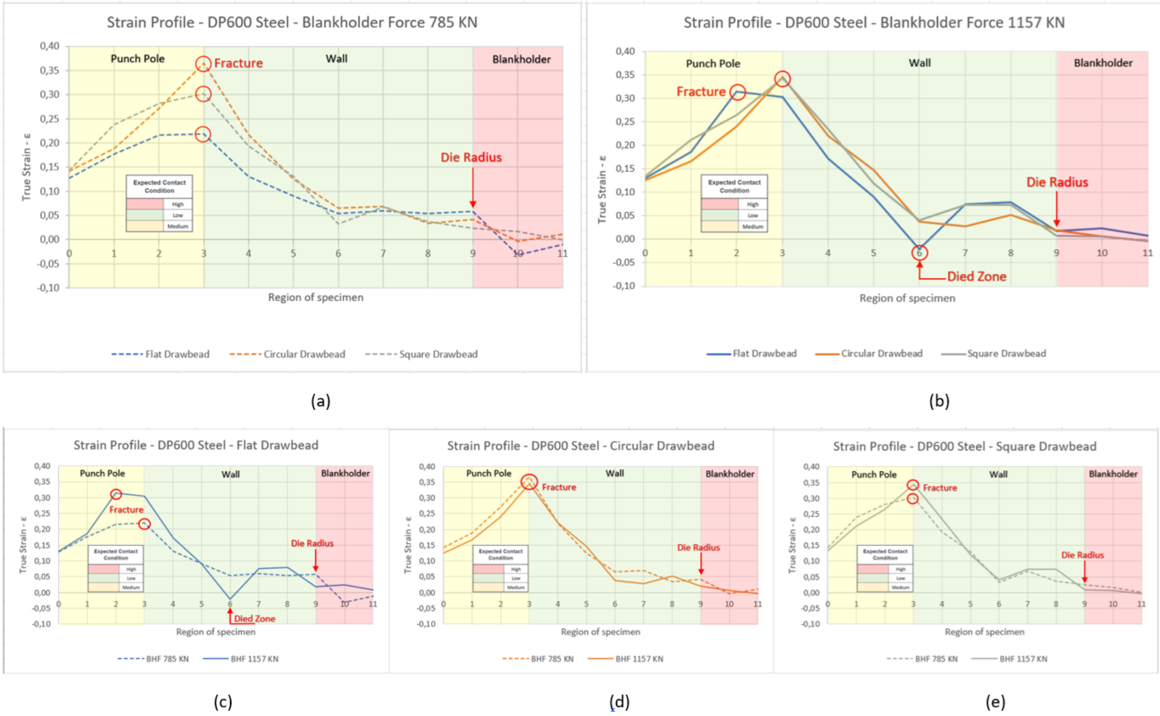

Figure9–Strain profile curves comparison to different blank holder forces and different drawbead geometries: (a) comparison to blank holder force of 785 kN, (b)comparison to blank holder force of1157 kN, (c) comparison to flat drawbead, (d) comparison to circular drawbead and (e) comparison to square drawbead.

The basic principle to be considered in the analysis of the graphs in Figure 9 is the variation of deformations in each region, from the flange to the punch pole. It is known that a greater variation of deformations between regions implies a more heterogeneous deformation condition of the sheet, that is, a less uniform condition of material flow, which leads to a greater concentration of stresses and, consequently, to a lower deformation until the sample cracks (lower formability). In this sense, both Figures 9(a) and 9(b) show a more uniform deformation profile for the circular drawbead, in both sheet press forces (785 kN and 1157 kN), which, in advance, already explains that the drawbead geometry presented better formability in the forming limit curves.

Regarding the circular drawbead, it can also be seen in Figure 9(d) that the deformation graphs for the sheet press forces of 785 kN and 1157 kN presented very similar profiles, which justifies the better formability of the circular DB in relation to the other DBs for both BHFs (according to Figure 6). The better performance of the circular DB with the 1157 kN BHF was due, to a large extent, to the smaller deformation generated by this BHF in the die radius (region 9), which implied a smaller deformation up to region 6 of the sample wall, causing less work hardening of the material at the beginning of the part wall region (transition region in the sheet deformation process, as discussed in section 3.3). This gain is attributed to the larger BHF used, since this is an analysis for the same drawbead geometry (circular).

For the square drawbead, a critical point in the deformation profile of the graphs in Figures 9(a) and 9(b) was region 6, on the wall of the stamped body. At this point, for both the 785 kN BHF and the 1157 kN BHF, there was less deformation of the material, that is, the previously increasing deformation profile decreased in region 6, compromising the less uniform variation of deformations in this section. This fact is attributed to the lower formability of the square DB in relation to the circular DB.

Comparing the performance of the square DB, for the 785 kN and 1157 kN BHFs (Figure 9(e)), it can be said that, as in the circular DB, there is a certain proximity between the deformation profiles, however, there is greater deformation on the radius of the die for the 785 kN force. Considering the better performance of the square DB with the BHF of 1157 kN, it is clear how important the deformation of the sheet metal over the die radius is (Bauschinger effect), indicating that a significant reduction in work hardening at this point results in a significant gain in the material's formability. It is worth highlighting again the positive effect of a greater force of the sheet metal press used.

Analyzing the deformation profiles for the flat DB, which represented the worst formability condition for DP600 steel, it is noted that the graphs (Figures 9(a), 9(b) and 9(c)) had the greatest variability of deformations between regions, i.e., this shows how important it is to use the DB in stamping operations to standardize the flow of the sheet. It is observed that the BHF of 785 kN was totally insufficient to stamp the material, causing a negative deformation in the flange. This negative deformation between the sheet press and the die is due to the BHF used being insufficient to contain the circumferential compressive stresses in the flange, responsible for the formation of wrinkles. This aspect compromised the forming of the sheet, since the maximum deformation at the breaking point, with BHF of 785 kN, was much lower than the deformation reached at this point with BHF of 1157 kN (Figure 9(c)). Furthermore, as shown in Figure 9(c), the deformation over the die radius with a BHF of 785 kN was also greater than that of a BHF of 1157 kN, making it catastrophic for the formability of the steel with a flat DB at this lower BHF.

Still regarding the flat DB, a very important fact to be observed was the formation of the so-called “dead zone” for the tests with a BHF of 1157 kN (Figures 9(b) and 9(c)). This defined the point on the graph over region 6, on the wall of the stamped cup, which presented convex curvature and negative deformation. This aspect was predominant for the worse formability of the flat DB, with a BHF of 1157 kN, in relation to the circular and square DBs. Although the 1157 kN BHF did not cause negative deformation in the flange, it was under this condition that the counterflow of the sheet, flowing in opposite directions from the flange and from the punch pole, most compromised the behavior of the material in the sample wall region, making it completely uneven. Thus, the formability of the DP600 steel, with flat drawbead and 1157 kN BHF, was superior only to the formability of this same drawbead with 785 kN BHF.

3.5 Hardness profile between concentric circles

Following the model for analyzing material deformations between the study regions, Vickers microhardness measurements were performed in these regions, since the deformations caused in each of them are directly related to the work hardening of the material during stamping. Thus, as in the measurement of deformations, it was possible to observe the variation in hardness of the sheet metal along the profile of the samples. The hardness reached by the material in each region suggests that the stresses resulting from the stamping process caused changes in the microstructure of the steel, proportional to its increase in hardness at each measured point.

Thus, similarly to Figure 9, Figure 10 presents the graphs of Vickers microhardness as a function of the regions defined by the concentric circles (0 to 11), printed on the surface of the 200 x 200 mm samples. The hardness curves were also grouped for the blank holder forces of 785 kN and 1157 kN, Figures 10(a) and 10(b), respectively, and subsequently for the flat, circular and square drawbeads, Figures 10(c), 10(d) and 10(e), respectively.

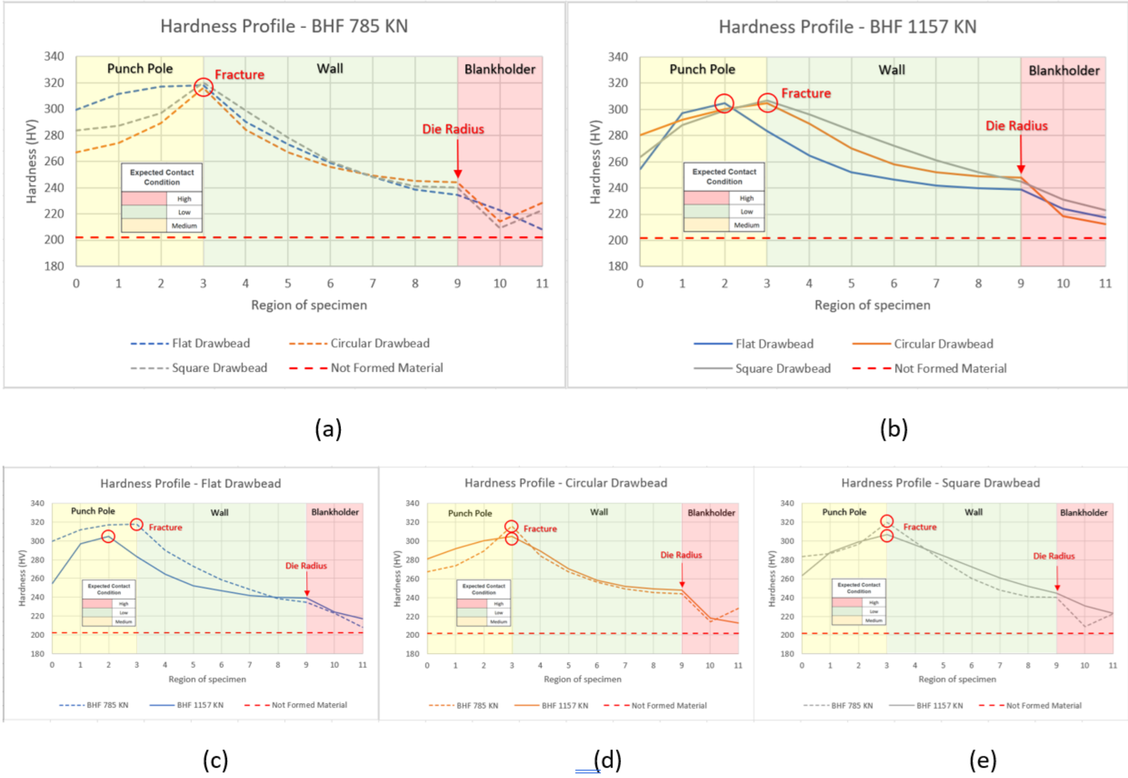

Figure10 –Hardness profile curves comparison to different blank holder forces and different drawbead geometries: (a) comparison to blankholder force of 785 kN, (b) comparison to blank holder force of1157 kN, (c) comparison to flat drawbead, (d) comparison to circular drawbead and (e) comparison to square drawbead.

A first characteristic observed in the graphs in Figures 10(a) and 10(b) was that, for all drawbead geometries, the hardness reached in the crack region was higher for the 785 kN BHF, with values close to 320 HV. For the 1157 kN BHF, the hardness in the crack region was close to 304 HV. This fact can be associated with a first explanation why for all drawbead geometries (flat, circular and square) the FLCs for the 785 kN BHF were lower than the FLCs for the 1157 kN BHF, as they concentrated a higher level of deformation in the most stressed region. Analyzing the flange region (9 to 11), for the 1157 kN BHF, the circular DB starts the profile (region 11) with lower hardness and the square DB with higher hardness. For all DBs, there is an increase in hardness up to the radius of the die (region 9). However, this hardness profile in the flange ends up impacting the hardness profile in the region of the sample wall (from region 9 to region 3), changing the profile variation for each DB geometry. This can also have a direct consequence on the results of the FLCs, in which the circular DB performed better than the square DB, which in turn performed better than the flat DB.

In the flange region, it should be noted that the circular and square DBs promote pre-deformation of the sheet before the punch acts, which does not occur with the flat DB, which does not have the "tooth". The flat DB, however, has a higher hardness at point 11 than the circular DB because, even without the tooth, there is a drag of the sheet under pressure between the die and the blank press, hardening the material. For the square DB, the hardness at point 11 is the highest, due to the higher level of pre-deformation caused by the tooth geometry.

Still for the 1157 kN BHF, a different hardening profile is observed for each DB model. The square model presents a practically linear hardness profile, from the flange to the rupture point (from region 11 to region 3), with a higher hardness level along the wall of the test specimen, when compared to the other DB geometries. On the contrary, the flat DB presents the lowest hardness level than the others along the wall of the test specimen, due to the dead zone formed in region 6, shown in the graph of the sheet deformation profile. In addition to the lower hardness level, this caused the crack to move to deformation region 2, while the circular and square geometries presented the crack in region 3.

For the 785 kN BHF, the work hardening profile along the sheet wall is much closer between the different DBs, with all presenting the crack in region 3. In this BHF, a different hardness profile is evident in the flange region, with a progressive increase in hardness for the flat DB (uniform flow in contact with the die and press-plate), while for the circular and square DBs there is a negative variation from region 11 to 10 and a subsequent increase in hardness from region 10 to 9 (die radius). In the die radius, a greater hardening is also noted for the circular DB and less for the flat DB.

This hardness in region 9, which characterizes the Bauschinger effect in sheet metal stamping, was favorable to the circular DB, since the total variation in hardness from this point (244 HV) to the breaking point (316 HV) was 72 HV, i.e., lower than the flat and square DBs. The flat DB presented a hardness of 240 HV at point 9 and 320 HV at point 3, i.e., a variation of 80 HV, while the flat DB presented a hardness of 234 HV at point 9 and 318 HV at point 3, with a hardness variation of 84 HV along the wall of the part.

This variation in hardness on the wall of the test specimen, however small, causes a relevant impact on the stampability of the material, since stamping is very sensitive to variations in tooling parameters (adjustments). Proof of this is shown by the results of the FLCs obtained with the 785 kN BHF, whose best performance was, again, that of the circular DB, and the worst performance of the flat DB.

Because of the variation in hardness in the flange and wall of the stamped sample, there is a variation in the hardening profile in the region of the punch pole. In all cases, the variation in hardness was negative from the crack region (3) to the punch pole (0). For the 1157 kN BHF, a much sharper drop in hardness is noted for the flat DB and a smaller one for the circular DB. It is understood that a greater variation in hardening between regions corresponds to a more heterogeneous (less uniform) deformation condition, concentrating more stresses between regions and, therefore, detrimental to the formability of the sheet. In view of this analysis, the best performance of the circular DB and the worst performance of the flat DB through the FLCs for the 1157 kN BHF are justified once again.

For the 785 kN BHF, where there is a higher hardness peak in the crack region, the greater reduction in hardness at the punch pole characterizes a stress relief due to plastic deformation, which was greater in the circular DB and smaller in the flat DB, given that the curve profile is opposite to the curve profile for the 1157 kN BHF. In this case, the better performance of the circular DB and the worse performance of the flat DB for the 785 kN BHF is once again justified.

This hardness peak in the crack region for the 785 kN BHF, greater than the maximum hardness reached for the 1157 kN BHF, is a preponderant factor for the better stamping performance of the sheet with the 1157 kN BHF, in relation to the 785 kN BHF, a fact that occurred for all DB geometries.

3.5.1 Hardness variation in the wall region

Given the importance of the wall region of the stamped body in the formability of DP600 steel, this section sought to analyze the work hardening of the material in this region, specifically between points 3 and 9 of the previous graphs (Figure 11).

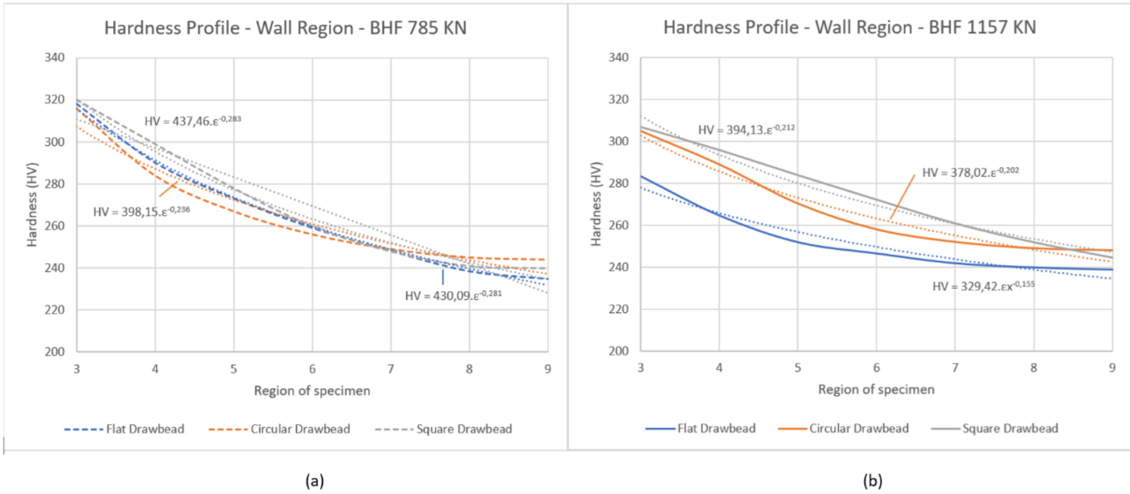

Figure11 – Hardness profile curves of the wall region of the stamped samples to (a) 785 kN blank holder force and (b) 1157 kN blank holder force.

Considering that the wall region of the specimen is practically free of friction, consequently, it is the one with a stress state closest to the uniaxial one imposed on specimens subjected to tensile tests. In this way, it can be said that the equation resulting from the hardness profile of this region resembles the Holloman/Ludwig equation, whose exponent refers to the material hardening coefficient. The profile equations referring to each drawbead geometry and blank holder force used present strain hardening exponents with values close to the strain hardening exponent of DP600 steel (n = 0.2209). Therefore, the variation in this value for each profile generated is because of the variation in BHF and DB used to harden the material during stamping.

The closest approximation of values occurred for the square and circular DBs, with BHF of 1157 kN, with exponent values of 0.212 and 0.202 respectively. For the BHF of 785 kN, it can be said that the circular DB presented a good approximation of the exponent value (0.236) to the hardening coefficient value (0.2209), however, for the flat and square DB's, the exponent values of the equations were the highest, 0.281 and 0.283, respectively. This indicates that, for the BHF of 785 kN, the flat and square DB's showed greater work hardening in the region of the sample wall, directly affecting the formability of the DP600 steel in this test configuration, as indicated by the FLC's of the material under study.

In conventional tensile testing, a higher work hardening coefficient indicates better drawability by stretching the material. For stamping tests, however, this condition does not necessarily imply better drawability, since the FLCs indicate the opposite, that is, worse drawability under these conditions. This is since a lower BHF induces the sheet to the drawing deformation mode, in addition to which, the effect of work hardening on the flange and the punch pole must be evaluated simultaneously, as they directly impact the sheet's response to stamping. There is also the formation of a critical zone at the beginning of the sample wall, after the die radius, which also affects the plastic behavior of the material during deformation.

3.6 Hardness vs. true strain

Based on the graphs representing the deformation and hardness profiles of DP600 steel, for the regions delimited by the concentric circles, a relationship was established between these variables, for the region of the wall of the stamped test specimen, as shown in Figure 12. Once again, the graphs were grouped for the sheet holder forces of 785 kN and 1157 KN, Figures 12(a) and 12(b), respectively and subsequently, for the flat, circular and square drawbeads, Figures 12(c), 12(d) and 12(e), respectively.

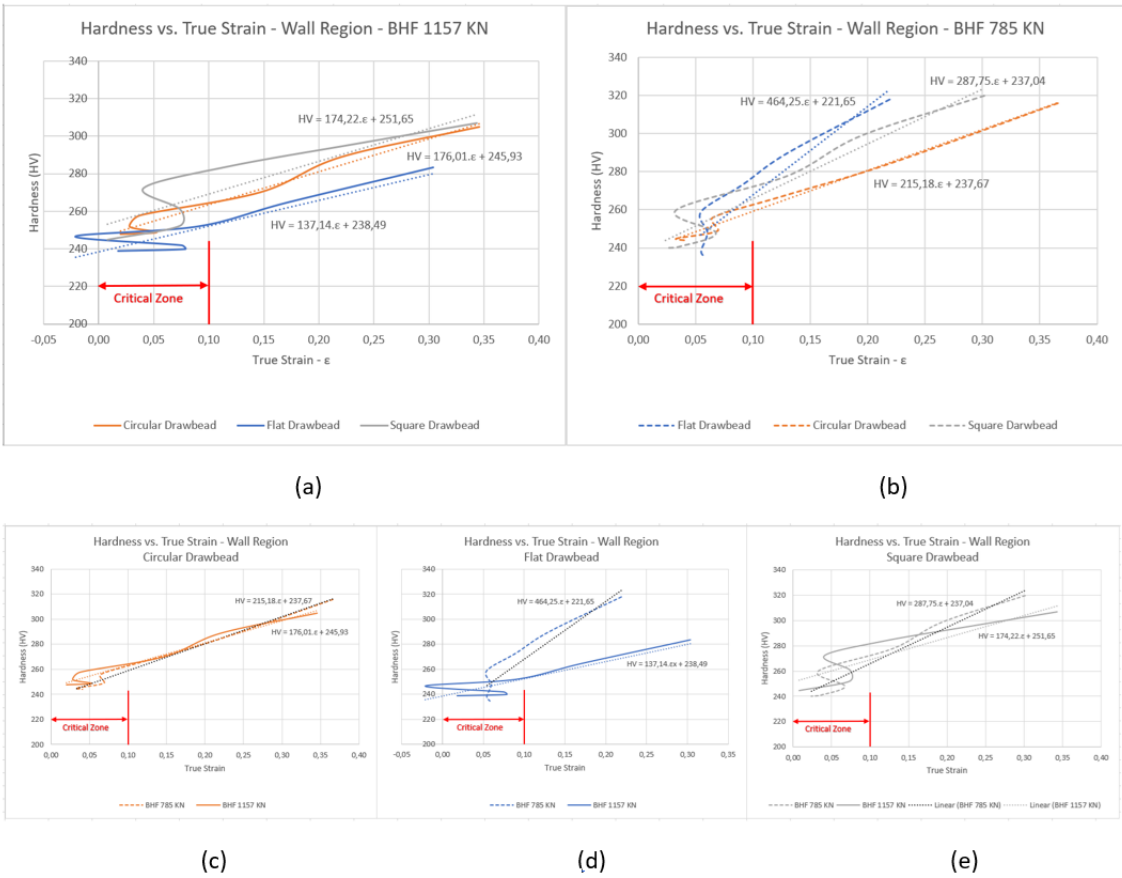

Figure12 - Hardness vs. True strain curves of the wall region of the stamped samples to (a) 785 kN blank holder force, (b) 1157 kN blank holder force, (c) circular drawbead, (d) flat drawbead and (e) square drawbead.

All graphs in Figure 12 show a zone of instability of deformations, defined as the “critical zone” of the sheet, since the hardness curves present a uniform and increasing profile, mainly in the region of the wall of the test specimen. This zone of instability occurs from the radius of the die (region 9) to the inside of the wall of the sample, up to region 6, for both blank holder forces used, 785 kN and 1157 kN.

According to the graphs of Hardness vs. True Deformation, the zone of instability of deformations causes a sharp variation in true deformation (horizontal direction) and hardness (vertical direction), between regions 9 and 6. The curves resulting from the use of the circular drawbead were those that presented the smallest variation, both in deformation and hardness. For the flat drawbead, there was a large variation in deformation for the BHF of 1157 kN and a large variation in hardness for the BHF of 785 kN, whereas for the square drawbead, there was a significant variation in both deformation and hardness for both blank holder forces.

Analyzing then the zone of deformation instability, at the beginning of the sheet wall formation, it can be said that the circular DB was the model that remained more stable, since both variations (deformation and hardness) were smaller than those presented by the Flat and square DB's. Considering then that the FLC's with circular DB were the ones with the best stampability, this better stability at the beginning of the formation of the part wall is associated with a better distribution of deformations along the rest of the wall up to the crack region, resulting in a less compromise of the formability of the sheet due to hardening during plastic deformation of the metal.

It can also be said that, for the circular DB, there is a better balance in terms of BHF variation, due to the proximity of the curves with 785 and 1157 kN (Figure 12(c)). For the flat DB there was the greatest discrepancy between the curves at 785 and 1157 kN of BHF, which justifies the worse performance for this drawbead.

Comparing the deformation vs. hardness curves for each BHF used, for the 1157 kN BHF, the three DB geometries presented a lower angular coefficient, i.e., a lower increase in hardness/deformation, in relation to the curves obtained with the 785 kN BHF. In relation to the FLCs, it can be said that this condition favored the performance of the DP600 steel with 1157 kN BHF, since for the three DB geometries, the FLC with this BHF presented better formability for the DP600 steel.

For each curve represented, the graphical interpretation of the material's behavior in the critical zone is complex to analyze, making it necessary to carry out in-depth studies for a more detailed representation of this aspect. Regardless of this, trend lines with linear functions were added to the graphs to characterize, in an approximate way, the behavior of the sheet in the wall region. Through these extracted functions, a comparative analysis of experimental results and results from numerical simulation will become possible, in order to provide a refinement of existing numerical models.

4. CONCLUSIONS

The results obtained in this study demonstrated the crucial influence of the blank holder force (BHF) and the drawbead (DB) geometry on the formability of DP600 steel. As expected, the forming limit curves revealed that both the applied BHF and the DB design directly affect the formability of the material. It is worth highlighting the circular geometry drawbead and the force of 1157 kN, which provided the best stamping performance for the steel used. The worst performance occurred for the tests with the flat drawbead, i.e., without the tooth.

In view of these results, this study proposed an analysis methodology using concentric circles printed on the surfaces of the samples, which proved to be an efficient analysis tool, and this is the main conclusion of the work. This model demonstrated, through the deformation and hardness profiles of the stamped material, how the variables “blank holder force” and “drawbead geometry” affect the plastic behavior of the steel during stamping in different deformation regions, conclusively explaining the results obtained through the forming limit curves.

Other conclusions:

The analysis of the deformation profile in different regions of the material highlighted the importance of the combination between the BHF and the geometry of the drawbead in obtaining more homogeneous deformations, which directly affects the quality of the stamping. Therefore, precise control, based on a more sophisticated knowledge of these parameters, is essential for optimizing the stamping processes.

The analyses carried out based on the concentric circles highlighted the importance of understanding the mechanical behavior of the material in different regions during the process, as this allows precise adjustments that enhance the efficiency of the forming process.

According to the results, in addition to balancing the flow of material in the flange (brake), the drawbead also has the function of preventing the formation of a dead zone, which impairs the formability of the material, making the deformation more heterogeneous.

The correlation between the variation in deformation and hardness defined functions that represent the effect of the BHF and the geometry of the DB in the wall region of the stamped test specimens, which can be applied to numerical simulation models to make them more accurate.

The way in which the CCM (Concentric Circles Method) is used in the modified Nakazima stamping tests allows it to be replicated in practical operations in the industry, by printing equidistant lines on the surface of the blanks, following the design of the die and punch.

5. REFERENCES

1. Keeler SP (1965) Determination of forming limits in automotive stampings. Sheet Met Ind 42:683–691
2. Goodwin GW (1968) Application os strain analyses to sheet metal forming problems in the press shop. Metall Italiana 60:764–774
3. Woodthorpe J, Pearce R (1969) The efect of r and n upon the forming limit diagrams of sheet metal. Sheet Metal Ind 1061–1067
4. ISO 12004–2 (2008) Metalic materials - sheet and strip - determination of forming-limit curve. European Committe for Standardization
5. HINO, Ryutaro; YASUHARA, Satoki; FUJII, Yutaka; HIRAHARA, Atsushi; YOSHIDA, Fusahito. Forming Limits of Several High-Strength Steel Sheets under Proportional/Non-Proportional Deformation Paths. **Advanced Materials Research**, [S.L.], v. 939, p. 260-265, 7 maio 2014. Trans Tech Publications, Ltd.. http://dx.doi.org/10.4028/www.scientific.net/amr.939.260.
6. PAN, Li Bo; ZHU, Hong Chuan; LEI, Ze Hong; ZHANG, Zhi Jian. Experimental Researches on Nonlinear Strain Paths Forming for Dual Phase Steel. **Advanced Materials Research**, [S.L.], v. 1004-1005, p. 209-213, 13 ago. 2014. Trans Tech Publications, Ltd.. http://dx.doi.org/10.4028/www.scientific.net/amr.1004-1005.209.
7. SCHWINDT, Claudio D.; STOUT, Mike; IURMAN, Lucio; SIGNORELLI, Javier W.. Forming Limit Curve Determination of a DP-780 Steel Sheet. **Procedia Materials Science**, [S.L.], v. 8, p. 978-985, 2015. Elsevier BV. http://dx.doi.org/10.1016/j.mspro.2015.04.159.

8. CARDOSO, Marcelo Costa; PEREIRA, Alexandre de Melo; SILVA, Fabiane Roberta Freitas da; MOREIRA, Luciano Pessanha. Experimental Analysis of Forming Limits and Thickness Strains of DP600-800 Steels. **Applied Mechanics And Materials**, [S.L.], v. 835, p. 230-235, maio 2016. Trans Tech Publications, Ltd.. http://dx.doi.org/10.4028/www.scientific.net/amm.835.230.

9. PAUL, Surajit Kumar. Controlling factors of forming limit curve: a review. **Advances In Industrial And Manufacturing Engineering**, [S.L.], v. 2, p. 100033, maio 2021. Elsevier BV. http://dx.doi.org/10.1016/j.aime.2021.100033.

10. FROHN-SÖRENSEN, Peter; NEBELING, Daniel; REUTER, Jonas; ENGEL, Bernd. A Critical Evaluation of Forming Limit Curves Regarding Layout of Bending Processes. **Key Engineering Materials**, [S.L.], v. 926, p. 1051-1060, 22 jul. 2022. Trans Tech Publications, Ltd.. http://dx.doi.org/10.4028/p-d09adu.

11. OLIVEIRA, Alex Raimundo de; LAJARIN, Sérgio Fernando; REBEYCA, Claudimir José; CHEMIN FILHO, Ravilson Antonio; NIKHARE, Chetan P.; MARCONDES, Paulo Victor Prestes. Influence of drawbead geometry and blank holder force on the dual phase steel formability. **The International Journal Of Advanced Manufacturing Technology**, [S.L.], v. 121, n. 9-10, p. 5823-5833, 19 jul. 2022. Springer Science and Business Media LLC. http://dx.doi.org/10.1007/s00170-022-09603-4.

12. SANRUTSADAKORN, Apichat; LAWONG, Winai; JULSRI, Weerapong. Numerical Study of Predicting Forming Process Based on Different Hardening Models in Advanced High Strength Steel Sheets. **Key Engineering Materials**, [S.L.], v. 951, p. 21-32, 7 ago. 2023. Trans Tech Publications, Ltd.. http://dx.doi.org/10.4028/p-g0pkwh.

13. REZAZADEH, V.; HOEFNAGELS, J.P.M.; GEERS, M.G.D.; PEERLINGS, R.H.J.. On the critical role of martensite hardening behavior in the paradox of local and global ductility in dual-phase steels. **European Journal Of Mechanics - A/Solids**, [S.L.], v. 104, p. 105152, mar. 2024. Elsevier BV. http://dx.doi.org/10.1016/j.euromechsol.2023.105152.

14. ABEYRATHNA, Buddhika; ROLFE, Bernard; HODGSON, Peter; WEISS, Matthias. A first step towards a simple in-line shape compensation routine for the roll forming of high strength steel. **International Journal Of Material Forming**, [S.L.], v. 9, n. 3, p. 423-434, 18 abr. 2015. Springer Science and Business Media LLC. http://dx.doi.org/10.1007/s12289-015-1238-7.

15. KE, Junyi; LIU, Yuqi; ZHU, Hongchuan; ZHANG, Zhibing. Formability of sheet metal flowing through drawbead – an experimental investigation. **Journal Of Materials Processing Technology**, [S.L.], v. 254, p. 283-293, abr. 2018. Elsevier BV. http://dx.doi.org/10.1016/j.jmatprotec.2017.11.051.

16. SCHMID, Harald; HETZ, Peter; MERKLEIN, Marion. Failure behavior of different sheet metals after passing a drawbead. **Procedia Manufacturing**, [S.L.], v. 34, p. 125-132, 2019. Elsevier BV. http://dx.doi.org/10.1016/j.promfg.2019.06.129.

17. BARLO, Alexander; SIGVANT, Mats; ENDELT, Benny. On the Failure Prediction of Dual-Phase Steel and Aluminium Alloys Exposed to Combined Tension and Bending. **Iop Conference Series**: Materials Science and Engineering, [S.L.], v. 651, n. 1, p. 012030, 1 nov. 2019. IOP Publishing. http://dx.doi.org/10.1088/1757-899x/651/1/012030.

18. SARAND, Mohammad Hasan Joudivand; MISIRLIOGLU, I. Burc. A physics-based plasticity study of the mechanism of inhomogeneous strain evolution in dual phase 600 steel. **International Journal Of Plasticity**, [S.L.], v. 174, p. 103918, mar. 2024. Elsevier BV. http://dx.doi.org/10.1016/j.ijplas.2024.103918.

19. KHAN, Muhammad Shehryar; SOLEIMANI, Maryam; MIDAWI, Abdelbaset R.H.; ADERIBIGBE, Isiaka; ZHOU, Y. Norman; BIRO, Elliot. A review on heat affected zone softening of dual-phase steels during laser welding. **Journal Of Manufacturing Processes**, [S.L.], v. 102, p. 663-684, set. 2023. Elsevier BV. http://dx.doi.org/10.1016/j.jmapro.2023.07.059.

20. RAJAK, Bijoy; KISHORE, Kaushal; MISHRA, Vipin. Investigation of a novel TIG-spot welding vis-à-vis resistance spot welding of dual-phase 590 (DP 590) steel: processing-microstructure-mechanical properties correlation. **Materials Chemistry And Physics**, [S.L.], v. 296, p. 127254, fev. 2023. Elsevier BV. http://dx.doi.org/10.1016/j.matchemphys.2022.127254.

21. CHENG, Nuo; YANG, Shanglei; LI, Yanlei; ZHAO, Xinlong; BI, Junhang; TIAN, Jiawei. Analysis of fatigue fracture mechanism of laser spiral welding of dissimilar metals of 6082 high strength aluminum alloy and DP980 high strength dual phase steel. **Materials Today Communications**, [S.L.], v. 41, p. 110665, dez. 2024. Elsevier BV. http://dx.doi.org/10.1016/j.mtcomm.2024.110665.

22. MANSUR, Vinicius Machado; MANSUR, Raquel Alvim de Figueiredo; CARVALHO, Sheila Medeiros de; SIQUEIRA, Rafael Humberto Mota de; LIMA, Milton Sergio Fernandes de. Effect of laser welding on microstructure and mechanical behaviour of dual phase 600 steel sheets. **Heliyon**, [S.L.], v. 7, n. 12, p. 1-100, dez. 2021. Elsevier BV. http://dx.doi.org/10.1016/j.heliyon.2021.e08601.

23. PARK, Myeong-Heom; FUJIMURA, Yuto; SHIBATA, Akinobu; TSUJI, Nobuhiro. Effect of martensite hardness on mechanical properties and stress/strain-partitioning behavior in ferrite + martensite dual-phase steels. **Materials Science And Engineering**: A, [S.L.], v. 916, p. 147301, nov. 2024. Elsevier BV. http://dx.doi.org/10.1016/j.msea.2024.147301.

24. MENG, Bao; WAN, Min; WU, Xiangdong; YUAN, Sheng; XU, Xudong; LIU, Jie. Inner wrinkling control in hydrodynamic deep drawing of an irregular surface part using drawbeads. **Chinese Journal Of Aeronautics**, [S.L.], v. 27, n. 3, p. 697-707, jun. 2014. Elsevier BV. http://dx.doi.org/10.1016/j.cja.2014.04.015.

25. FOLLE, Luis Fernando; SCHAEFFER, Lirio. Avaliação das condições tribológicas em estampagem de chapas através do ensaio de dobramento sob tensão. **Matéria (Rio de Janeiro)**, [S.L.], v. 22, n. 2, p. 1-100, 2017. FapUNIFESP (SciELO). http://dx.doi.org/10.1590/s1517-707620170002.0141.

26. VOTAVA, Filip; JIRKOVÁ, Hana; KU?EROVÁ, Ludmila; JENÍ?EK, Št?pán. Study of Transition Areas in Press-Hardened Steels in a Combined Tool for Hot and Cold Forming. **Materials**, [S.L.], v. 16, n. 1, p. 442, 3 jan. 2023. MDPI AG. http://dx.doi.org/10.3390/ma16010442.

27. ZHANG, Yong; ZUO, Ting Ting; TANG, Zhi; GAO, Michael C.; DAHMEN, Karin A.; LIAW, Peter K.; LU, Zhao Ping. Microstructures and properties of high-entropy alloys. **Progress In Materials Science**, [S.L.], v. 61, p. 1-93, abr. 2014. Elsevier BV. http://dx.doi.org/10.1016/j.pmatsci.2013.10.001.

28. MA, Hongyue *et al*. A virtual laboratory based on full-field crystal plasticity simulation to characterize the multiscale mechanical properties of AHSS. **Scientific Reports**, [S.L.], v. 12, n. 1, p. 1-100, 23 mar. 2022. Springer Science and Business Media LLC. http://dx.doi.org/10.1038/s41598-022-09045-8.

29. LIMA, Renan de Melo Correia; TOLOMELLI, Flávia Tereza dos Santos Fernandes; CLARKE, Amy J.; CLARKE, Kester D.; SPADOTTO, Julio Cesar; ASSUNÇÃO, Fernando Cosme Rizzo. Microstructural characterization of a 1100 MPa complex-phase steel. **Journal Of Materials Research And Technology**, [S.L.], v. 17, p. 184-191, mar. 2022. Elsevier BV. http://dx.doi.org/10.1016/j.jmrt.2021.12.106.

30. WEBBER, Eli; KNEZEVIC, Marko. Assessing strength of ferrite and martensite in five dual phase and two martensitic steels via high throughput nanoindentation to elucidate origins of strength. **Journal Of Materials Research And Technology**, [S.L.], v. 33, p. 3635-3648, nov. 2024. Elsevier BV. http://dx.doi.org/10.1016/j.jmrt.2024.10.054.

31. KATIYAR, Lokendra Kumar. Enhancing mechanical properties and wear resistance of dual phase steel through surface mechanical attrition treatment. **Results In Surfaces And Interfaces**, [S.L.], v. 17, p. 100332, out. 2024. Elsevier BV. http://dx.doi.org/10.1016/j.rsurfi.2024.100332.

32. SHEN, Fu Hui; WANG, He Song; XU, Hao; LIU, Wen Qi; MÜNSTERMANN, Sebastian; LIAN, Jun He. Local Formability of Different Advanced High Strength Steels. **Key Engineering Materials**, [S.L.], v. 926, p. 917-925, 22 jul. 2022. Trans Tech Publications, Ltd.. http://dx.doi.org/10.4028/p-dds916.

33. LIMA, Tiago N.; CALLEGARI, Bruna; FOLLE, Luís Fernando; SANTOS, Ygor Tadeu B. dos; ZAMORANO, Luiz Gustavo; SILVA, Bruno Caetano dos S.; COELHO, Rodrigo Santiago. Microstructural Evolution of a Hot-Stamped Boron Steel Automotive Part and Its Influence on Corrosion Properties and Tempering Behavior. **Materials Research**, [S.L.], v. 26, p. 1-100, 2023. FapUNIFESP (SciELO). http://dx.doi.org/10.1590/1980-5373-mr-2022-0494.

34. NENE, Saurabh S.. Microstructure and Mechanical Properties of High Entropy Alloys. **High Entropy Alloys**, [S.L.], p. 99-175, 2024. Springer Nature Singapore. http://dx.doi.org/10.1007/978-981-99-7173-2_4.

35. PEREIRA, Rui; PEIXINHO, Nuno; COSTA, Sérgio L.. A Review of Sheet Metal Forming Evaluation of Advanced High-Strength Steels (AHSS). **Metals**, [S.L.], v. 14, n. 4, p. 394, 28 mar. 2024. MDPI AG. http://dx.doi.org/10.3390/met14040394.

36. ZHANG, Y.; DUAN, Y.; MU, Z.; FU, P.; ZHAO, J.. Non-Associated Flow Rule Constitutive Modeling Considering Anisotropic Hardening for the Forming Analysis of Orthotropic Sheet Metal. **Experimental Mechanics**, [S.L.], v. 64, n. 3, p. 305-323, 21 fev. 2024. Springer Science and Business Media LLC. http://dx.doi.org/10.1007/s11340-024-01032-6.

37. TIPALIN, Sergey A.; BELOUSOV, Vladislav B.; SHPUNKIN, Nikolay F.. Investigation of Uneven Properties of Stainless Steel 12Kh18N10T Depending on the Thickness of the Sheet. **Defect And Diffusion Forum**, [S.L.], v. 410, p. 28-36, 17 ago. 2021. Trans Tech Publications, Ltd.. http://dx.doi.org/10.4028/www.scientific.net/ddf.410.28.

38. TRZEPIECI?SKI, Tomasz. Recent Developments and Trends in Sheet Metal Forming. **Metals**, [S.L.], v. 10, n. 6, p. 779, 10 jun. 2020. MDPI AG. http://dx.doi.org/10.3390/met10060779.

39. PEREIRA, A.F.G.; PRATES, P.A.; OLIVEIRA, M.C.; FERNANDES, J.V.. Inverse identification of the work hardening law from circular and elliptical bulge tests. **Journal Of Materials Processing Technology**, [S.L.], v. 279, p. 116573, maio 2020. Elsevier BV. http://dx.doi.org/10.1016/j.jmatprotec.2019.116573.

40. KRAIRI, Anouar; MARMI, Jalil; GASTEBOIS, Sabrina; VELDHUIS, Mark; KOTT, Matthäus. A Speed-up Method for Numerical Simulations of Multi-strokes Cold Metallic Sheet Forming Processes. **Procedia Manufacturing**, [S.L.], v. 47, p. 570-577, 2020. Elsevier BV. http://dx.doi.org/10.1016/j.promfg.2020.04.173.